ISSN 1068-3755, Surface Engineering and Applied Electrochemistry, 2024, Vol. 60, No. 2, pp. 194–203. © Allerton Press, Inc., 2024.
Russian Text © The Author(s), 2023, published in Elektronnaya Obrabotka Materialov, 2023, No. 5, pp. 1–11.

Composition, Structure, and Wear Resistance of Surface Nanostructures Obtained by Electric Spark Alloying of 65G Steel

E. V. Yurchenko[a, *], G. V. Ghileţchii[b], S. A. Vatavu[b], V. I. Petrenko[c, †], D. Harea[c], C. Bubulinca[d], and A. I. Dikusar[a, c, †]

[a] *Shevchenko Transnistrian State University, Engineering and Technical Institute, Tiraspol, 3300 Republic of Moldova*
[b] *Faculty of Physics and Engineering, Moldova State University, Chisinau, MD-2009 Republic of Moldova*
[c] *Institute of Applied Physics, Moldova State University, Chisinau, MD-2028 Republic of Moldova*
[d] *National Research and Development Institute for Cryogenic and Isotopic Technologies Rm. Valcea, Department of Energy, Ramnicu Valcea, 240050 Romania*
**e-mail: e.iurcenko@mail.ru*

Received January 30, 2023; revised March 6, 2023; accepted March 15, 2023

Abstract—A combination of X-ray diffraction and X-ray fluorescence analysis has shown that the strengthened layer formed during electric spark alloying of 65G steel with a processing electrode made of the T15K6 hard alloy is a nanocrystalline material, the ratio of the crystalline and amorphous phases in which is achieved by changing the discharge energy. Since an increase in discharge energy leads to an increase in surface roughness and its amorphization, there is an optimal value of discharge energy at which maximum wear resistance of the resulting nanocomposites is achieved. At $E = 0.2$ J, the wear resistance of the hardened layer is 7–10 times higher than the wear resistance of the untreated surface.

Keywords: electric spark alloying, nanocrystalline materials, tribology, wear resistance, 65G steel, hard alloy, carbides

DOI: 10.3103/S1068375524020145

INTRODUCTION

Among various methods of surface modification, such as electrodeposition, physical vapor deposition (PVD), magnetron and plasma sputtering, plasma-electrolytic saturation of the surface, etc., electric spark alloying (ESA) occupies a special place due to its advantages such as: (a) strong metallurgical connection between the modified surface and the original one; (b) high corrosion and wear resistance; (c) relatively low temperature influence and, as a consequence, minimal mechanical damage. The obvious advantages of the method include its simplicity, accessibility and relatively low cost of equipment and technology itself. The method is based on the use of transfer of anode material to the surface being treated by spark discharges in various environments: air, inert gas, dielectric liquid, etc., as well as in vacuum.

Technologists and researchers owe the origin of this method to engineers from the USSR, spouses B.R. and N.I. Lazarenko, as evidenced by their early publications dating back to the 1950s, as well as more recent ones [1, 2]. The use of electric spark modification of surfaces, initially steels, and subsequently a wide range of materials, provided an effective and economically sound solution to a number of technology problems: hardening the surface and increasing its wear resistance [1–3], increasing corrosion resistance [4, 5], and now also the production of biologically compatible surfaces [6]. As has been shown in a number of recent studies, surface nanostructuring occurs during ESA [7–18], which is achieved either naturally [7–9, 11, 16] or by inserting ultrafine material into the processing electrode (PE) [10, 12, 17, 18].

Moreover, based on experiments [19], when carbon nanotubes are used as PE, we can talk about the technical justification of nanoelectroerosion and electrical discharge processing of metamaterials and nanostructures [20]. Considering the fact that as a result of the ESA process, the resulting surfaces are nanocomposites [13, 19, 21], the composition of which is determined by both the PE material and the surface being processed, their properties are also largely determined by both the PE material and processed surface [22].

Recently, it seems obvious that nanostructuring of surface layers and the application of nanostructured coatings is an effective method for strengthening modern structural and instrumental materials. Using the concept of nanocrystalline materials [23], for which the volume of individual elements (grains) is less than

† Deceased.

Table 1. Work regimes of the Alier -31 installation

Regime	Pulse duration, μs, ±10%	Pulse amplitude, A, ±20%	Energy, J	Frequency, Hz, ±10%
1	16	125	0.036	3200
2	31	125	0.070	1600
3	62	175	0.200	800
4	125	175	0.390	400
5	250	175	0.790	200
6	500	175	1.580	100

Table 2. The chemical composition of OE and of the processed surface

	Fe	C	Si	Mn	W	Ti	Co
OE	–	–	–	–	79(WC)	15(TiC)	6
Steel 65G	98	0.6–0.7	0.17–0.37	0.8–1.2	–	–	–

the volume of the boundaries between them, it becomes possible to control the properties of surface layers based on nanostructuring. One of the methods for implementing this process is ESA.

The purpose of this work is to study the composition, structure, and properties of 65G steel, subjected to modification using ESA and using T15K6 hard alloy containing W and Ti carbides as a PE, and Co as a binder material. Since one of the main applications of this steel is the use as part of soil-cultivating machines, the change in the properties of the surface of the steel after its ESA modification was assessed by measuring its wear resistance depending on the modes of electric spark action. According to [24], ESL is one of the modern technologies that improves the wear resistance of soil-cultivating equipment. The study involved obtaining an answer to the main question of materials science: composition–structure–property in relation to the ESA modification of the steel under study, which, in turn, should provide effective methods for its processing.

SURFACE TREATMENT METHOD AND CHARACTERIZATION OF THE OBTAINED SURFACES

The processing was carried out using an installation for applying electric spark coatings Alier-31 (Scinti, Moldova), the use of which provided the processing modes presented in Table 1.

Using the above processing modes, the surfaces of samples made of 65G steel (GOST 1050–88) were modified, the chemical composition of which is presented in Table 2. The chemical composition of OE made from the T15K6 hard alloy is also given there.

The processing was carried out in automatic mode when the sample was moved relative to the PE at a speed of 0.16 mm/min. The total processing time for one sample was 8 min, which, with a sample size of 30 × 40 mm (1200 mm^2), provided a surface modification rate of 0.66 min/cm^2. The PE with an area of 2 × 2 mm^2 was fixed in a vibrator operating at the frequency presented in Table 1, depending on processing modes. In the process of surface modification, as the mass of the electron was produced, the distance between the rod and the sample was adjusted. The signal was a decrease in the intensity of spark discharges.

The coefficient of the PE material transfer to the sample (the ratio of the mass of the PE metal transferred in the form of a melt or during evaporation into the interelectrode gap to the mass of the material deposited on the substrate) averaged ~0.5 with an average error of ~17%. No noticeable effect of discharge energy on the transfer coefficient was found.

The elemental composition (wt.%) of the resulting composites was determined using X-ray fluorescence analysis (Xenemetrix, Israel). Light elements (carbon, oxygen, nitrogen) were not determined in the version of the method used. The analysis of surface layers was carried out to a depth of 3–5 μm.

The influence of the discharge energy was also assessed by measuring the surface roughness after its modification (R_z, μm) using a Surtronic profilometer (Taylor Hobson, UK). Standard deviations are given below as intervals.

The structure of the surface after its modification was studied using an Empyrean diffractometer (Malvern PANalytical, the Netherlands). Details of the analysis of the resulting diffraction patterns will be presented in Figs. 2 and 3.

Microstructural studies were carried out using a Carl Zeiss FESEM scanning electron microscope equipped with an EDX system.

The tribological properties of the samples were assessed on a Bruker UMT TriboLab device at 20°C

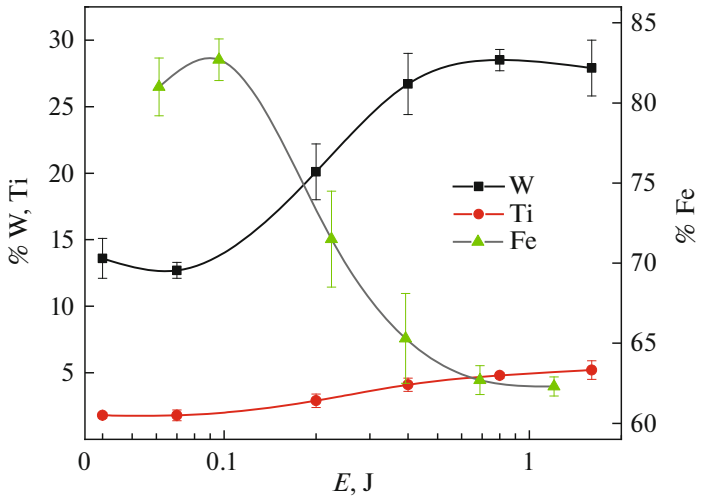


Fig. 1. Effect of discharge energy on the concentration of heavy elements in the coating after ESA.

using a ball-plane friction pair [25, 26] (silicon nitride ball diameter 3 mm, hardness HV > 12, density 3.2 g/cm^3, normal force 300 N and friction speed 0.015 m/s). The depth of the friction path was determined automatically.

RESULTS AND DISCUSSION

Composition and Structure of the Surface after ESA

During ESA, the PE material is transferred to the surface of the workpiece under conditions of spark discharges of varying intensity. As indicated above, the transfer intensity was assessed at different discharge energies by: (a) the relative value of mass transfer (by measuring the transfer coefficient—the ratio of the increase in the mass of the treated surface to the mass removed from the surface of the PE); (b) the results of X-ray fluorescence (XRF) (elemental) analysis, which fixes the concentration (essentially relative) of heavy elements of the PE transferred to the treated surface, as well as heavy elements of the treated surface; (c) the results of X-ray diffraction (XRD) analysis, which makes it possible to evaluate the composition and concentration of crystalline structures in the surface layer after ESA.

It is shown above that the transfer coefficient with the used version of the surface modification method did not change, within the measurement error, depending on the discharge energy. As for the elemental composition, according to the results presented in Fig. 1, with increasing discharge energy, an increase in the content of W and Ti carbides is observed (judging by the increase in the concentration of these elements) and a decrease in the concentration of the main component of steel (Fe). However, regardless of the discharge energy, this element formed the basis of the surface layer, since its concentration was ~60–80% (mass). The results presented in Fig. 1 do not answer the question about the structure of the phases of the surface layer (crystalline or amorphous), as well as their chemical composition (the presence of corresponding metals in the form of oxides of carbides or nitrides, for example).

Significant additional information can be obtained by using X-ray diffraction, the main results of which are shown in Figs. 2 and 3. The presented pattern were obtained by using an X-ray tube with CuK_α radiation at $\lambda = 1.54060$ Å in the θ–2θ configuration according to the following technique:

– in order to remove Fe and Ti fluorescence, an algorithm was used according to [27];

– to remove pattern caused by radiation diffraction, at $\lambda = 1.54439$ Å, we used the method described in [28];

– comparison of the positions of radiation maxima was carried out according to ICDD (PDF 4+, 2022);

– quantitative analysis was carried out using the Rietveld method in accordance with [29];

– to determine the size of crystallites, the modified Williamson–Hall method was used [30].

From the presented spectra it follows that, in contrast to the substrate (steel 65G), on the treated surface there are observed not only reflections caused by the PE material (W and Ti carbides), but also iron carbide ($Fe_{0.94}C_{0.06}$), as well as at low energy, a peak corresponding to crystalline carbon is recorded (Figs. 2, 3). It should also be noted that the reflex corresponding to WC (the main component of the PE) is present when treated with low discharge energy, but is absent when treated with a discharge energy of 1.56 J (Fig. 3). It seems obvious that during the ESA process, PE carbides are not only transferred to the surface being processed, but are also synthesized during its processing. In this case, the content of Fe carbide in crystalline form can not only exceed the content of Fe, but also

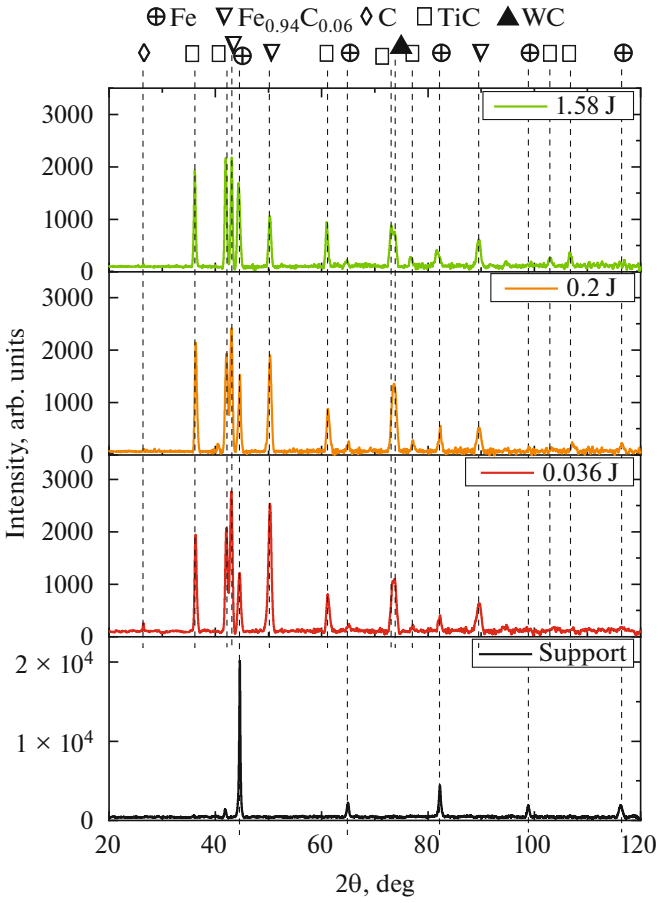


Fig. 2. Diffraction pattern of surfaces obtained at different discharge energies in comparison with the pattern of the substrate.

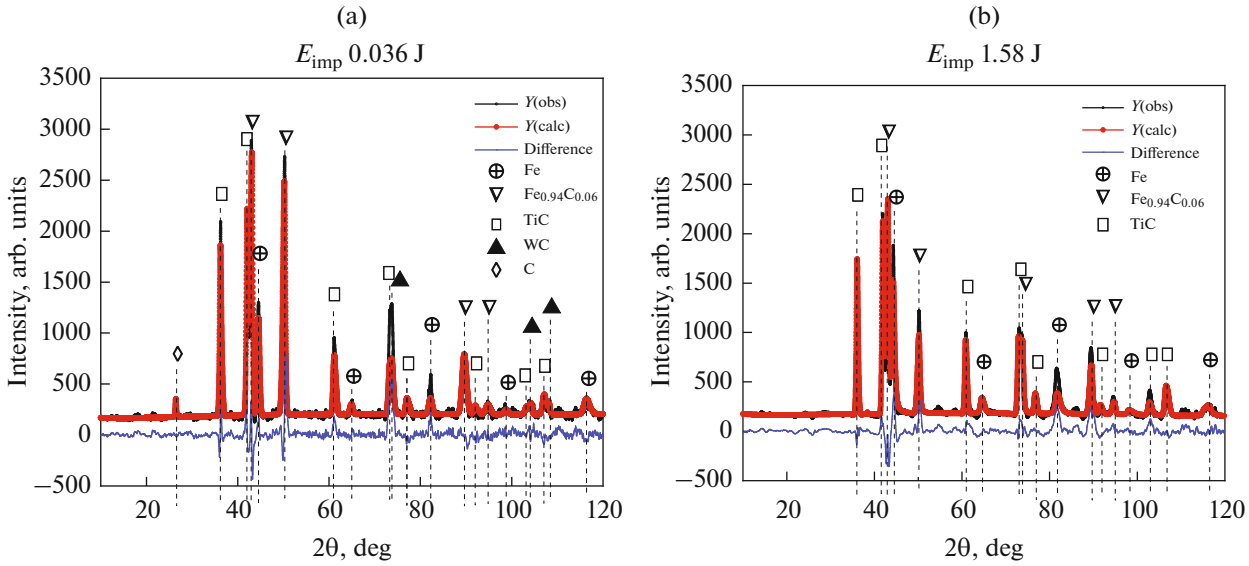


Fig. 3. Results of quantitative analysis of XRD pattern: an example of the application of the Rietveld method in X-ray diffraction analysis of samples obtained at discharge energies of 0.036 (a) and 1.58 J (b).

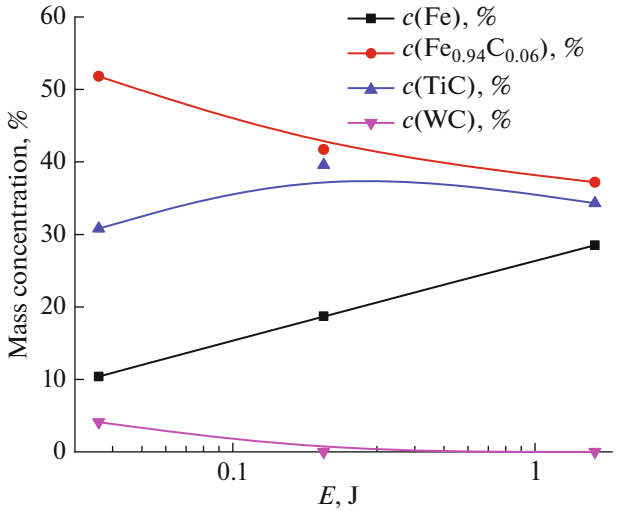


Fig. 4. The influence of discharge energy on the concentration of various crystalline forms of phases contained in the surface.

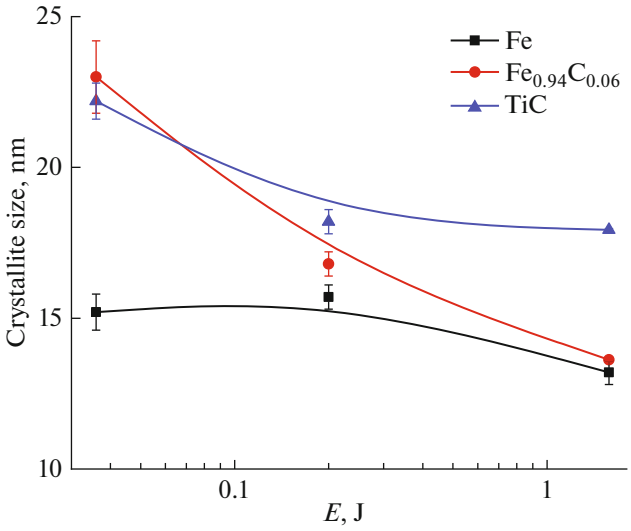


Fig. 5. Effect of discharge energy on crystallite sizes.

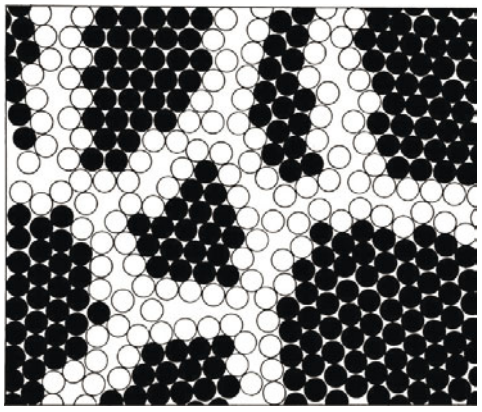


Fig. 6. Two-dimensional model of a nanostructured material. Atoms corresponding to the crystalline form of the material are shown as black circles. The boundary regions represented by white circles correspond to the amorphous phase [23].

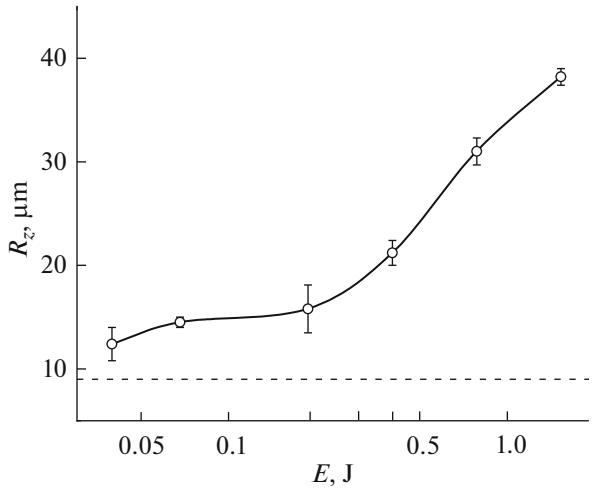


Fig. 7. Effect of discharge energy on surface roughness. The dotted line corresponds to the average roughness of the samples before ESA.

account for more than 50% by weight of all detected crystalline forms on the surface (Fig. 4).

However, as can be seen from the example of the main PE carbide, W carbide, when transferred under spark discharge conditions, a modification of its structure occurs (Figs. 1, 3), namely, its amorphization takes place. This is evidenced by several facts. First, a comparison of the results of elemental (Fig. 1) and X-ray phase (Fig. 4) analysis. If according to XRF results the W content is 15–30% (Fig. 1), then according to X-ray diffraction results it is no more than 5% (Fig. 4). It is absolutely obvious that a significant part of tungsten carbide, and it is possible that other tungsten compounds, is transferred to the coating in an amorphous state. Secondly, a significant decrease in the crystalline form of WC is observed with increasing discharge energy (Figs. 2–4). At the maximum used energy (1.56 J), there is no WC phase in the coating (Fig. 3), while the W concentration reaches ~30% (Fig. 1). That is, W is transferred, but in an amorphous rather than crystalline form. An assessment of the sizes of crystallites present in the surface in significant quantities shows that they correspond to the nanometric scale (Fig. 5).

Taking into account the above, we can conclude that the surfaces obtained during ESA are defined according to the classification [23] as a partially or completely nanostructured material. It can be represented schematically as shown in Fig. 6. These are crystalline phases of nanometric sizes, surrounded by an amorphous phase. At least for the WC phase (the

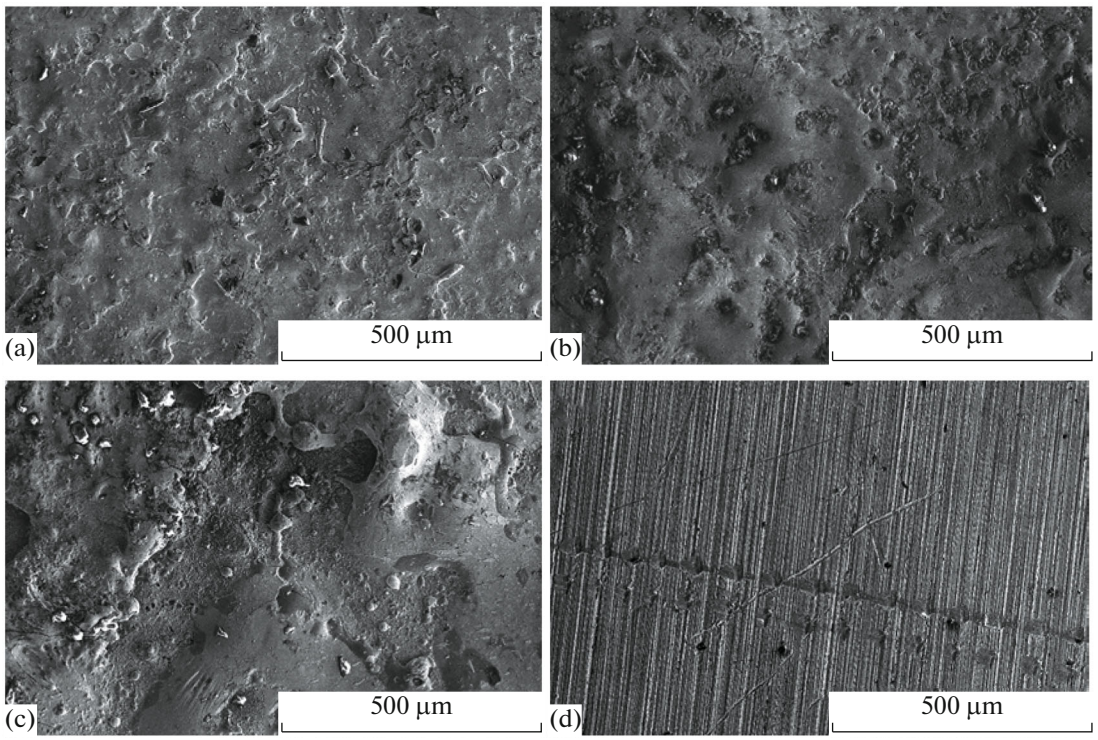


Fig. 8. Surface topology after treatment: at $E = 0.036$ J (a), at $E = 0.2$ J (b), at $E = 1.6$ J (c), substrate surface (d).

main phase of the PE) this has been established quite reliably.

Figure 7 presents the results of measuring surface roughness after ESA at different discharge energies (according to R_z). It is obvious that in all cases the roughness increases with increasing discharge energy. However, if at relatively low energies R_z increases insignificantly (for example, when the discharge energy increases from 0.036 to 0.2 J, the increase in R_z is ~30%), then at high energies it increases by 2.5 times (Fig. 7). The surface topography (Fig. 8) confirms the results of roughness measurements.

It is also necessary to emphasize that it is at high discharge energies that the degree of surface amorphization increases.

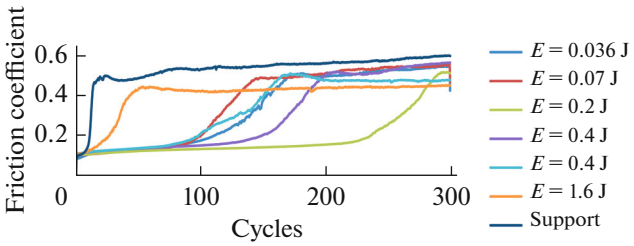


Fig. 9. Diagram of the friction coefficient depending on the number of friction cycles.

Tribological Test Results

The measurements of the wear of hard and superhard materials by friction is not always a trivial task. The difficulty is that friction pairs have similar or close mechanical parameters. In this case, the degree of wear of the material under study depends not only on the number of friction cycles, but also directly on the modification of the shape of the counterbody due to its wear. In this work, Si_3N_4 balls were used, which show a significant difference in wear resistance with the measured materials, which allows us to neglect the wear of the counterbody.

In general, the wear process of a friction pair consists of three periods—running-in, normal, and accelerated wear. The running-in process, which is based on complex mechanical, physical, and chemical processes, largely determines the overall wear resistance of parts. By the end of the running-in period, the main operational characteristics of the surface, such as roughness, micro-hardness, residual stresses, the structure of the metal boundary layer, and surface integrity, acquire optimal values corresponding to the given operating conditions. These conditions are determined by the material of the rubbing pairs, sliding speed, temperature in the contact zone, specific pressure, etc. At the beginning of the running-in period, the actual contact surface of the friction pair is only a small part of the calculated value, since contact occurs along the tops of microroughnesses, where large specific pressures develop. Under their action,

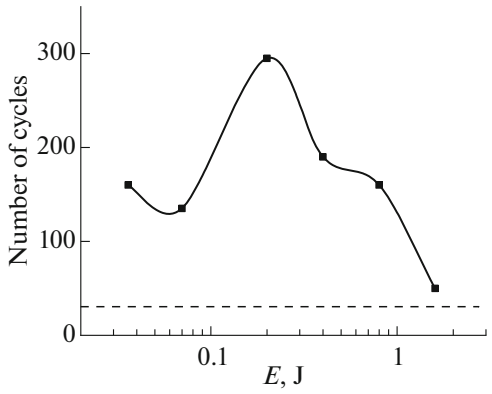


Fig. 10. Dependence of the number of cycles required for complete wear of the hardened layer on the discharge energy during ESA. The dotted line corresponds to the number of wear cycles on the untreated surface.

elasto-plastic deformation occurs at the contact points, leading to the formation of a new surface microprofile.

In this work, we used the method of continuous measurement of the friction coefficient over 300 cycles. The pressure between the friction pairs was achieved through the use of a relatively small ball diameter (3 mm) and a fairly large normal load (300 N), which led to rapid running-in of the friction contact. During the sliding cyclic interaction of Si_3N_4 balls with the surface under study, the friction coefficient diagram quite accurately showed the moment of wear of the hardened layer (Fig. 9). The moment of transition from the running-in period to the stage of normal wear in our case is characterized on the friction coefficient diagram by the transition to an increased friction coefficient and its relative stabilization. This moment means for hardened surfaces that the influence of the applied layers has been reduced to nothing.

All treated samples showed a significant increase in wear resistance compared to the untreated substrate surface. Thus, the untreated substrate "got in" in less than 30 cycles. The best result was shown by a sample modified by ESA at $E = 0.2$ J, which was ground in 295 cycles, which almost tenfold increases the operating time of parts strengthened using the method and parameters used to obtain the sample processed at $E = 0.2$ J. This is shown quantitatively in Fig. 10. It can be seen that a sharp increase in the degree of wear occurs with an increase in roughness when processing with energies exceeding 0.2 J (Fig. 7). Taking into account that an increase in discharge energy also leads to amorphization of the surface (Figs. 3, 4), we can conclude that the combination of these two factors leads to a significant decrease in wear resistance (Fig. 10).

Thus, with increasing of the application energy, on the one hand, the surface softens due to a decrease in the content of the crystalline phase and to an increase in the concentration of amorphous phases, on the other hand, the structured surface increases wear resistance to a certain limit.

The immersion of the ball into the test surface during friction (Fig. 11) showed that on all the obtained curves, with the exception of the curve for the substrate, a clear abrupt transition is visible, indicating a change in the immersion rate (that is, an increase in the wear rate). For clarity, this is shown by a dashed line on the curve of the sample obtained at a discharge energy of 0.8 J. It should be noted that the transition region corresponds to the beginning of the normal wear region on the friction coefficient diagram (Fig. 9). It is also obvious that the maximum wear resistance is demonstrated by the surface treated at $E = 0.2$ J. In this case, the counterbody deepened by only 0.020 mm over 300 friction cycles, which is significantly lower in comparison with the untreated substrate, which showed a deepening of 0.075 mm. In terms of the volume of material removed, taking into account the track length of 1 cm, we obtain a sevenfold reduction in the volume of material removed by friction, processed under the above optimal alloying conditions, in comparison with the substrate.

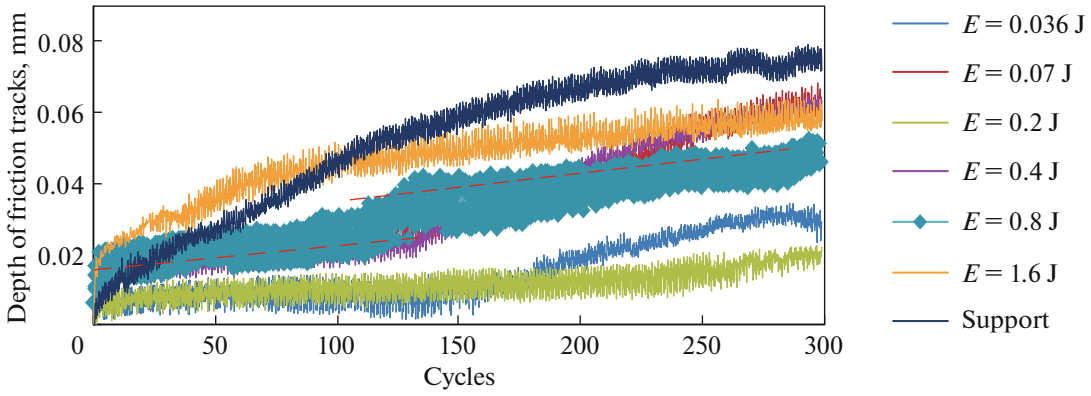


Fig. 11. The depth of friction tracks depending on the number of cycles.

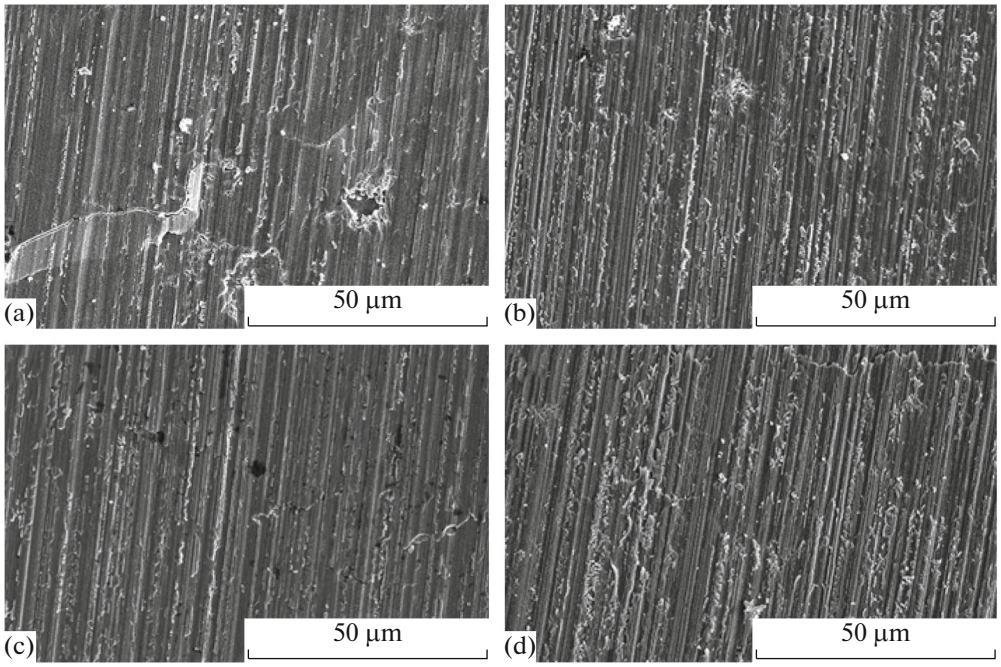


Fig. 12. Surfaces obtained after 300 friction cycles and at different discharge energies, J: 0.2 (a), 0.4 (b), 0.8 (c), 1.6 (d).

One should also pay attention to the fact that for surfaces processed at high discharge energies, that is, amorphized and at the same time having high roughness, in the initial period of friction the depth of the track may even exceed that achieved for the substrate (Fig. 11).

Microscopic Analysis of Friction Surfaces

Microphotographs of surfaces obtained during ESA with different discharge energies after tribological tests are presented in Fig. 12.

The surfaces obtained at minimum and maximum discharge energies after frictional contact with the balls (Figs. 12a, 12d) represent regions with densely packed wear residues [31]. The remaining samples showed the presence of so-called corrugated wear with a small amount of residue. The minimum amount of residues is expectedly observed on the friction surface of the surface sample obtained at $E = 0.2$ J (Fig. 12a).

CONCLUSIONS

Using the example of ESA of 65G steel with a processing electrode made of T15K6 hard alloy, a combination of X-ray phase and XRF analysis of the surface shows that its modification, accompanied by the transfer of PE material, is at the same time a method for obtaining a nanocrystalline material, the ratio of the concentration of the amorphous and crystalline phases, in which it is possible to control the energy category. Wherein:

– a significant part of the crystalline phase is iron carbide, synthesized during processing;

– crystallite sizes are within the nanometric scale;

– the degree of surface amorphization increases with increasing discharge energy.

The combination of an increase in surface roughness and its amorphization with an increase in charge energy during ESA is the reason that an optimum discharge energy is observed, at which maximum wear resistance is achieved:

– when using various methods for assessing wear resistance (the number of friction cycles until the hardened layer is completely removed and assessing the depth of the track during friction), it is shown that maximum wear resistance is achieved with a discharge energy of 0.2 J;

– under the above ESA conditions, the wear resistance of the modified layer increases by 7–10 times in comparison with the untreated surface.

FUNDING

This work was carried out within the framework of funding from the ANCD project (Moldova) No. 20.80009.5007.18 Manufacturing of new micro- and nanostructuring materials by physicochemical methods and the elaboration on their base, as well as budget funding from the Pridnestrovian State University. T.G. Shevchenko, as well as with the support of the ANCD project (Moldova) No. 20.80009.5007.12 and the CaRISMA center (Centrul Regional Interdisciplinar Ştiinţifico-Educaţional pentru Studiul Materialelor Avansate) of the Faculty of Physics and Engineering.

CONFLICT OF INTEREST

The authors of this work declare that they have no conflicts of interest.

REFERENCES

1. Lazarenko, B.R. and Lazarenko, N.I., *Elektro-iskrovyi sposob izmeneniya svoistv iskhodnykh poverkhnostei* (Electro-Spark Method for Changing the Properties of Original Surfaces), Moscow: Izd. Akad. Nauk SSSR, 1958.
2. Lazarenko, N.I., *Elektroiskrovoe legirovanie metallicheskikh poverkhnostei* (Electric Spark Alloying of Metal Surfaces), Moscow: Mashinostroenie, 1976.
3. Rukanskis, M., Control of metal surface mechanical and tribological characteristics using cost effective electrospark deposition, *Surf. Eng. Appl. Electrochem.,* 2019, vol. 55, no. 5, p. 607.
4. Chernova, G.P., Tomashov, N.D., Fedoseeva, T.A., et al., Increasing the corrosion resistance of alloys by applying coatings to them using the electrospark alloying method, *Elektron. Obrab. Mater.,* 1977, no. 4, p. 42.
5. Cao, G., Zhabg, X., Tang, G., and Ma, X., Microstructure and corrosion behavior of Cr coating on M50 steel fabricated by electrospark deposition, *J. Mater. Eng. Perform.,* 2019, vol. 28, no. 7, p. 4086.
6. Tang Chang-bin, Liu Duo-xin, Wang Zhan, and Gao Yang, Electro-spark alloying using graphite electrode on titanium alloy surface for biomedical applications, *Appl. Surf. Sci.,* 2011, vol. 257, c. 6304.
7. Yurchenko, V.I., Yurchenko, E.V., Fomichev, V.M., et al., Obtaining nanowires under conditions of electrodischarge treatment with Al–Sn alloy, *Surf. Eng. Appl. Electrochem.,* 2009, vol. 45, no. 4, p. 259.
8. Dikusar, A.I., Obtaining nanowires under conditions of electrodischarge treatment, in *Nanowires—Implementations and Applications,* Abbas Hashim, Ed., Rijeka, Croatia: IntechOpen, 2011, ch. 16, p. 357.
9. Nicolenco, S.V., Nanostructuring a steel surface by electrochemical treatment with new electrode materials based on tungsten carbide, *Surf. Eng. Appl. Electrochem.,* 2001, vol. 47, no. 4, p. 217.
10. Levashov, E.A., Minina, E.S., Sematullin, B.R., et al., Features of the influence of nanocrystalline powders on the structure and properties of Ti-C-40% KhN70Yu obtained by the SHS method, *Fiz. Met. Metalloved.,* 2003, vol. 95, no. 6, p. 38.
11. Topala, P., Ojegov, E. and Ursaki, V., Nanostructures obtaining using electric discharges at atmospheric pressure, in *Nanostructures and Thin Films for Multifunctional Applications,* Tigineanu, I., Topala, P., Ursaki, V., Eds., Cham: Springer, 2016, p. 43.
12. Zamulaeva, E.I., Levashov, E.A., Kudryashov, P.V., et al., Electrospark coatings deposited onto an Armco Iron substrate with nano-and microstructured WC–Co electrodes: Deposition process, structure and properties, *Surf. Coat. Technol.,* 2008, vol. 202, p. 3715.
13. Kuptsov, E.A., Sheveyko, A.N., Zamulaeva, E.I., et al., Two-layer nanocomposite WC/a-C coatings produced by a combination of a pulsed arc evaporation and electrospark deposition in vacuum, *Mater. Design,* 2019, vol. 117, p. 107645.
14. Nicolenco, S.V., Burkov, A.A., Dvornik, M.I., et al., Effect of parameters of electric spark discharge on the physico-chemical characteristics of steel 45 surface after the ESA electrodes based on WC–8% Co with chromium carbide additives, *Surf. Eng. Appl. Electrochem.,* 2019, vol. 55, p. 251.
15. Levashov, E.A., Kudryashov, A.E., and Potapov, N.T., New SHS materials for electric spark alloying using ultrafine powders, *Izv. Vyssh. Uchebn. Zaved., Tsvetn. Metall.,* 2000, no. 6, p. 67.
16. Parkansky, N., Beilis, I., Rapoport, L., et al., Electrode erosion and coatings properties in pulsed air arc WC-based hard alloys, *Surf. Coat. Technol.,* 1998, vol. 105, p. 130.
17. Kudryashov, A.E., Zamulaeva, E.I., Levashov, E.A., et al., Application of electrospark deposition process and modified SHS electrode materials to improve the endurance of hot mill rolls. Part 1. Features of coating formation on SPHN-60 white cast Iron substrate, *Surf. Eng. Appl. Electrochem.,* 2019, vol. 55, no. 4, p. 390.
18. Kudryashov, A.E., Zamulaeva, E.I., Levashov, E.A., et al., Application of electrospark deposition process and modified SHS electrode materials to improve the endurance of hot mill rolls. Part 2. Structure and properties of the formed coatings, *Surf. Eng. Appl. Electrochem.,* 2019, vol. 55, no. 5, p. 502.
19. Dai, H., Hafner, J., Rinzler, A., Colbert, D., et al., Nanotubes as nanoprobes in scanning probe microscopy, *Nature,* 1996, vol. 384, p. 147.
20. Slobodyan, S.M., Nanoelectroerosion: Correction of the effect of "SWCNT-Electrode," *Surf. Eng. Appl. Electrochem.,* 2021, vol. 57, no. 6, p. 627.
21. Kroitoru, D.M., Silkin, S.A., Kazak, N.N., et al., Physico-mechanical and tribological properties of carbon-containing nanocomposites produced by electrospark alloying, *Surf. Eng. Appl. Electrochem.,* 2021, vol. 57, no. 6, p. 617.
22. Ben'kovskii, Yu.V., Kroitoru, D.M., Petrenko, V.I., et al., Influence of steel composition on the properties of a composite surface obtained by electric spark alloying, *Elektron. Obrab. Mater.,* 2022, vol. 58, no. 1, p. 1.
23. Gleiter, H., Nanostructured materials: Basic concepts and microstructure, *Acta Mater.,* 2000, vol. 48, no. 1, p. 1.
24. Aulov, V.F., Luzhnykh, P.V., Kireinov, A.V., et al., Results of field tests of hardening of working bodies of soil-cultivating machines, in *Trudy Vserossiiskogo nauchno-issledovatel'skogo tekhnologicheskogo instituta remonta i ekspluatatsii mashinno-traktornogo parka GOSNITI* (Proceedings of the All-Russian Scientific Research Technological Institute for the Repair and Operation of Machine and Tractor Park GOSNITI), Moscow, 2013, vol. 113, p. 300.

25. Harea, E., Stoček, R., Storozhuk, L., Sementsov, Yu., et al., Study of tribological properties of natural rubber containing carbon nanotube and carbon black as hybrid filler, *Appl. Nanosci.,* 2019, vol. 9, p. 899.

26. Harea, E., Stoček, R., and Machovsky, M., Study of friction and wear thermoplastic vulkanuzates: The correlation with abraded surfaces topology, *J. Phys.: Conf. Ser.,* 2017, vol. 843, p. 012070.

27. Someveld, E.J. and Visser, J.W., Automatic collection of powder data from photographs, *J. Appl. Cryst.,* 1975, vol. 8, p. 1.

28. Rachinger, W.A., A correction for α1; α2 doublet in the measurement of widths of X-ray diffraction lines, *J. Sci. Instrum.,* 1948, vol. 25, p. 254.

29. Hill, R.J. and Howard, C.J., Quantitative phase analysis from powder diffraction data using the Rietveld method, *J. Appl. Cryst.,* 1987, vol. 20, p. 467.

30. Langford, J.L., The use of the Voigt function in determining microstructural properties from diffraction data by means of pattern decomposition, in *Accuracy in Powder Diffraction II,* Prince, E.O. and Stalick, J.K., Eds., NIST Special Publ. 846, Washington: US Dep. Commerce, 1992, p. 110.

31. Harea, E., Lapsker, I., Laikhtman, A., and Rapoport, L., Bauschinger's effect and dislocation structure under friction of LiF single crystals, *Tribol. Lett.,* 2013, vol. 52, no. 2, p. 205.

Publisher's Note. Allerton Press remains neutral with regard to jurisdictional claims in published maps and institutional affiliations.